frontiers | Frontiers in Materials

TYPE Original Research
PUBLISHED 26 September 2022
DOI 10.3389/fmats.2022.1003556

OPEN ACCESS

EDITED BY
Lei Wang,
Xi'an University of Architecture and Technology, China

REVIEWED BY
Jie Xiao,
Guangdong University of Technology, China
Gunasekaran Murali,
Peter the Great St.Petersburg Polytechnic University, Russia

*CORRESPONDENCE
Zhen Li,
lizhen@yangtzeu.edu.cn

SPECIALTY SECTION
This article was submitted to Structural Materials,
a section of the journal
Frontiers in Materials

RECEIVED 26 July 2022
ACCEPTED 17 August 2022
PUBLISHED 26 September 2022

CITATION
Shi P, Li Z, Chen X, Zeng L and Hu R (2022), Effect of industrial waste molecular sieves on internally cured cement-based materials.
Front. Mater. 9:1003556.
doi: 10.3389/fmats.2022.1003556

Effect of industrial waste molecular sieves on internally cured cement-based materials

Peng Shi[1], Zhen Li[1,2]*, Xiaorun Chen[3], Lei Zeng[1] and Rong Hu[4]

[1]School of Urban Construction, Yangtze University, Jingzhou, China, [2]School of Intelligent Construction, Wuchang University of Technology, Wuhan, China, [3]China Western Construction Academy of Building Materials Co., LTD, Chengdu, China, [4]Hubei Chufeng Jianke Group Jingzhou Kaiyuan New Materials Limited by Share LTD, Jingzhou, China

Using waste molecular sieves (MS) instead of sand as water-absorbing fine aggregates in cement-based materials can effectively deal with factory adsorption waste and reduce sand consumption. In this article, the industrial waste molecular sieve is recycled and incorporated into cement-based materials. The effect of the molecular sieve as a hydration internal curing agent on the performance of cement-based materials is studied. A series of experiments are designed to find out the appropriate ratio and to evaluate and analyze the internal curing effect of waste molecular sieves. Compressive strength, flexural strength, and dry shrinkage properties of mortar with different dosages of the molecular sieve are tested. The water release behavior of the molecular sieve in mortar is comprehensively analyzed combined with the desorption test of the molecular sieve. Results show that the compressive and flexural strength increase by 5% and 10%, respectively, and the drying shrinkage decrease by 6% when 10% of sand is replaced by a molecular sieve under the same total water content. The hydration behavior of the sample is characterized by a microcosmic test of paste. Thermogravimetric analysis is used to calculate the content of corresponding hydration products and quantitatively describe the hydration degree of the internal curing paste mixed with MS. Results show that the content of hydration products is improved by the addition of the molecular sieve, which provides a theoretical basis for the enhancement of mortar to a certain extent.

KEYWORDS

internal curing, strength, drying shrinkage, hydration degree, thermogravimetric analysis

Introduction

Internal curing technology has been extensively and systematically studied due to the improvement on concrete properties. Internal curing can effectively reduce the reduction of internal humidity of cement-based materials, reduce dry shrinkage cracks, and prevent acid corrosion on concrete surfaces (Liu et al., 2017; Xu et al., 2021). In addition, the internal curing technology can also promote the hydration of

cement-based materials, fill the pores of the slurry, and improve the strength and durability of concrete.

Commonly used internal curing materials include lightweight aggregate (PLA) (Bentur et al., 2001; Ghourchian et al., 2013; Balapour et al., 2019), highly absorbent polymers (SAP) (Jensen and Lura, 2006; Ye et al., 2012; Justs et al., 2015), and the superfine powder, such as rice husk ash (RHA) (Van et al., 2014), burnt grass ash (Lv et al., 2019), and cellulose fiber (Kawashima and Shah, 2011). Igarashi and Watanabe (2006) added SAP to concrete with a water–cement ratio of 0.25, and the self-shrinkage was significantly decreased. However, SAP leaves a large number of holes inside the concrete after absorbing and releasing water, which negatively affects the strengthening properties of the concrete (Justs et al., 2015). RHA has no negative effect on the strength of concrete, but the curing efficiency is limited by low water absorption (Antunes et al., 2019).

At present, the common water-absorbing light aggregates are pumice (Pietro et al., 2004), expanded shale (Zhuang et al., 2016), and perlite (Ranjbar, 2013). The water desorption performance of the water-absorbing aggregate itself plays an important role in the internal curing process. Also, Bentz and Weiss (2011) showed that an effective internal curing agent should not only have high water absorption capacity but also have high water release capacity at high relative humidity. There are already relevant standards for testing the water absorption rate and water release rate under different humidity levels. The curing efficiency of the internal curing agent in concrete is closely related to the particle size, water absorption, and pore size of the porous lightweight aggregate, and the performance of concrete will also be changed by these factors (Yang et al., 2021). The internal curing agent with a suitable particle size can be fully dispersed in the cement-based material, which can increase the effective curing area. Excessive porosity in the internal curing agent can lead to a decrease in the strength of the cement-based material, while small porosity will limit water absorption and affect curing efficiency. Therefore, there is an appropriate dosage for water-absorbent lightweight aggregates in cement-based materials. Also, Bentz et al. (2005) developed a relationship to obtain the required mass of PLA to replace the natural aggregates.

A molecular sieve is a crystalline aluminosilicate composed of a silicon–oxygen tetrahedron or aluminum–oxygen tetrahedron connected by oxygen bridges to form a molecular-sized channel and cavity system. It is widely used in the adsorption and separation process of the petrochemical industry and the removal of SO_2 and NO_x from industrial flue gas due to its unique sieving molecules and catalytic functions (Pujado et al., 1992; Fajula and Plee, 1994; Kulkarni, 1998). A large number of hydroxyl groups on the surface of the molecular sieve make the molecular sieve have stronger adsorption to water molecules. Thus, the water absorption of the molecular sieve will not be affected by the internal industrial waste gas, which enables the waste molecular sieve to be recycled as an internal curing agent. The pore size of molecular sieves is generally nanoscale. Among several industrial waste molecular sieves, the 13X type molecular sieve is selected as the internal curing agent in this project due to its large pores. Compared with other lightweight aggregates, the 13X molecular sieve has a small particle size and uniform distribution, which can be evenly distributed in cement-based materials, which is beneficial to improve the curing efficiency of internal curing agents.

The possible use of industrial adsorption waste as an internal curing agent for cement-based materials was explored in this article. In order to find a suitable way in mortar mixed with MS, mortar specimens with different dosages of wet MS were designed, and their compressive strength, flexural strength, and dry shrinkage properties were tested. To evaluate the curing efficiency of the MS for cement-based materials, the water release capacity of the MS under different relative humidity levels was tested by a desorption experiment. The hydration behavior of the sample was characterized by a microcosmic test of paste. Thermogravimetric analysis was used to calculate the content of corresponding hydration products and quantitatively describe the hydration degree of internal curing paste mixed MS. The purpose of this article is to incorporate industrial adsorption waste into concrete to achieve the purpose of recycling industrial waste. This study provides a theoretical basis for the application of waste in engineering and is of great significance in reducing environmental pollution.

Materials and methods

Raw materials

The mineral composition and physical properties of Portland cement (Grade 42.5) used in this study are shown in Tables 1, 2. Sand conforming to GB/T 17671-1999 standards is selected for this study. The particle size and pore size of 13X MS are 1 mm and 0.9 nm, respectively, according to the information provided by the manufacturer. A microscopic cross-sectional image of molecular sieves is shown in the Supplementary Material. The particle size distribution of sand and MS used in the experiment is shown in the Supplementary Material. The crushing strength of the molecular sieve is 60 N. The XRD pattern and the image of 13X MS are shown in Figures 1, 2, respectively. The XRD pattern matches well with PDF#12-0246, and 13X MS is mainly composed of sodium silicate aluminate. The MS is saturated after absorbing water for 1 h, and the water absorption rate of MS is 66.7%.

TABLE 1 Chemical composition of cement.

Composition	SiO_2	$Al2O_3$	Fe_2O_3	CaO	MgO	SO_3	Na_2Oeq	f-CaO	C_3S	C_2S	C_3A
Content (%)	21.36	5.20	3.68	64.57	1.70	0.97	0.56	0.80	57.55	17.82	7.54

TABLE 2 Physical properties of cement.

Fineness %	Specific surface area m^2/kg	Density kg/m^3	Standard consistency %	Loss %
0.4	354	3120	24.6	1.76

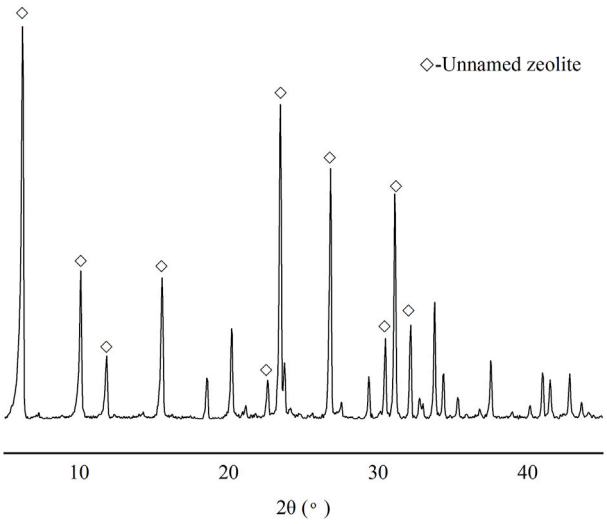

FIGURE 1
XRD pattern of the molecular sieve.

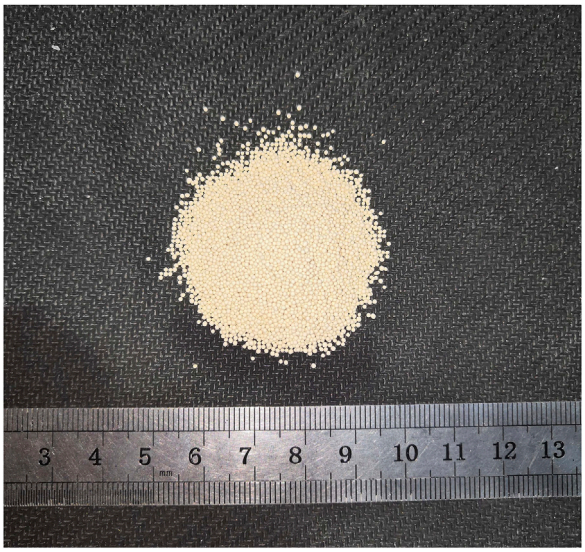

FIGURE 2
Image of the molecular sieve.

Experimental program

Mixture design

The strength contrast experiment of mortar was designed to find out the proper usage of industrial adsorption waste. The mix proportion for the strength test is shown in Table 3. Initial water–cement ratios of M0, IB15, and IS15 were kept constant at 0.5, and the sand-to cement-ratios were kept at 3.0. Part of the sand in the mixture was replaced by the same volume of MS. This method of incorporation was called the internal mixing method. Correspondingly, the method of adding MS to the mixture without replacing the sand was called the external mixing method. Mortars IE15 and IS15 with an MS volume replacement ratio of 15% were designed to analyze the influence of blank and saturated MS on strength. Considering that the total water–cement ratio would increase due to extra water, TIS10, TIS15, and TIS20 mortars with the same total water content and volume replacement rates of 10%, 15%, and 20% were poured. Meanwhile, in order to compare the effect of the internal mixing method and the external mixing method, a control group TES15 with the same total water content and 15% MS was set up. Six specimens were made for each set of mortar.

Relatively few studies have been performed on drying shrinkage of mortars with a constant total water content after adding additional water. According to strength values of different proportions, it was found that the mixing ratio with a constant total water content after adding additional water was more suitable for MS. Thus, mortars with the same total water

TABLE 3 Mix ratio of mortar.

Group	C (g)	W (g)	WE (g)	S (g)	MS (g)
M0	450	225	0	1350	0
IB15	450	225	0	1148	45
IS15	450	225	30	1148	45
TIS15	450	195	30	1148	45
TES15	450	195	30	1350	45
TIS10	450	205	20	1215	30
TIS20	450	185	40	1018	60

a) WE is for the extra water stored in the MS; b) In the symbol of mortar, the total water content is the sum of the water content and the extra water content, and "T" means that the total water content is the same as M0. "I" and "E" represent internal and external mixing methods, respectively, "B" and "S" represent blank molecular sieve and saturated molecular sieve, respectively; c) The number represents the volume dosage, for example, "15" means the volume dosage is 15%.

TABLE 4 Mix ratio of cement.

Group	C (g)	W (g)	WE (g)	MS (g)
P0	603	241	0	0
P15	603	241	24	37
TP15	603	217	24	37

content (M0, TIS10, TIS15, and TIS20) were selected for the drying shrinkage test. Also, the effect of MS content on the drying shrinkage of mortar was investigated.

To explore the micro properties of cement-based materials mixed with MS, three groups of cement pastes with dimensions of 40 mm × 40 mm × 40 mm were designed. W/B required for cementitious materials in the ideal hydration state was 0.42 (Jensen and Hansen, 2001). The initial water–cement ratio W/C was determined to be 0.4 by combining the empirical formula of Eq. 1. Here, W_e/C was the extra water binder ratio in the internal curing agent, and W/C was the initial water binder ratio.

$$W_e/C = \begin{cases} 0.18*W/C, W/C \le 0.36, \\ 0.42 - W/C, \ 0.36 \le W/C \le 0.42. \end{cases} \quad (1)$$

P0 was the control group without MS. The cement paste mixed with 15% volume content of water-saturated MS was named P15. Similar to the mortar, a group of pure paste TP15 with the same total water content and a molecular sieve volume content of 15% is added. The mixing ratio of cement paste is shown in Table 4.

Mixing procedure

Specimens of mortar and paste were mixed using a mortar mixer and a paste mixer at room temperature, respectively. Raw MS was immersed in water for 1 h in advance. The mixing process of mortar is shown as follows to solve the early release of water in cement: *1*) add cement and water to the sand cylinder of the mixer in advance, and start the mixer at low speed for 30 s after adding water and cement; *2*) add MS and sand to the mixture and continue beating at low speed for 30 s; *3*) all mixtures were mixed at high speed for 60 s. For specimens of cement paste, the mixing produce is shown as follows: *1*) fill the mixer with water and cement, and start the mixer on low speed for 30 s; *2*) add MS and continue beating at low speed for 90 s; *3*) all mixtures were mixed at high speed for 120 s.

Test methods

Water desorption

Curing efficiency is not only related to water absorption but also the desorption capacity at high RH of MS (Álvaro et al., 2021). Six different relative humidity (RH) conditions were created to study the desorption behavior of MS, which contained RH of 97%, 93%, 85%, 81%, 75%, and 59%. The relative humidity of different salt solutions is shown in Table 5. Salt solutions of K_2SO_4, KNO_3, KCl, KBr, NaCl, and NaBr were placed in the box for 24 h until the different equilibrium RH were reached (Zou et al., 2018). The desorption test device is shown in the Supplementary Material. Some studies have shown that procedures, where particles are dried with wet paper, are preferred (Dixit et al., 2019). The MS have been immersed in water for 24 h, and a wet paper towel was used to suck up the surface moisture in this project. The desorption test experimental device conforms to ASTM-E104 (2012). The glass dishes, used to hold MS, were placed in a box 24 h in advance until they reached a weight balance at different relative humidity levels. Mass of samples at 59% RH were measured every 1 h, and the other samples were weighed at a corresponding time. The ambient temperature was controlled at 21 ± 1°C.

Compressive strength and flexural strength of mortar

Mortar was cast into a mold with a size of 40 mm × 40 mm × 160 mm. A plastic film was applied to the mold immediately to prevent loss of water. Specimens were demolded after curing for 1 day in the mold with the plastic film and cured for 28 days at a temperature of 20°C with a relative humidity greater than 90%. Compressive and flexural strength of specimens were tested in accordance with the GB/T 17671-1999 (National Standard of the People's Republic of China, 2004). Each value was the average strength of the three test blocks. The compressive strength was measured on a press machine with a loading capacity of 300 KN. The test loading rate for compressive strength was 2.4 kN/s. The flexural strength of cement mortar was measured by the flexural testing machine.

TABLE 5 Relative humidity of different salt solutions.

Salt solution	K_2SO_4 (%)	KNO_3 (%)	KCl (%)	KBr (%)	NaCl (%)	NaBr (%)
RH	97	93	85	81	75	59

Dry shrinkage test

The dry shrinkage value was tested by the contact method, which was based on JGJ/T70-2009 (National Standard of the People's Republic of China, 2009). Shrinkage values of mortar with a size of 40 mm × 40 mm × 160 mm were measured on the BC-176 vertical mortar shrinkage tester. In addition, special molds in accordance with JGJ/T70-2009 were used, and special copper nails were cast in both ends of the mixture to observe the change in the length of specimens.

A plastic film was used to cover molds to prevent water loss of mixtures, and molds were removed from specimens after curing for 3 days to prevent the copper nails from moving in the mortar during demolding and measurement. Then, the specimens were transferred to a dry environment with a temperature of 20°C and relative humidity of less than 60%. The length of the specimen at the early stage of drying shrinkage was measured once a day and extended to 2 days in the late stage of dry shrinkage. Three test blocks were poured for each group of samples, and the dry shrinkage value was obtained from the average value of the three test blocks. The method to dry the shrinkage expansion rate is as follows:

$$\varepsilon_t = \frac{L_0 - L_t}{L - L_d}, \tag{2}$$

in which ε_t is the shrinkage rate of natural drying at t days, L_0 is the initial length of the specimen after molding for 3 days (mm), L_d is the sum of the length of two copper nail heads embedded in the mortar, i.e., 20 mm, L_t is the length of the specimen measured at t days (mm), and L is the specimen length, 160 mm.

X-ray diffraction

Influence of MS on the phase composition of the cement paste in the late stage of hydration was investigated by the X-ray diffraction analysis (XRD). After curing for 28 days, the specimens were crushed, and the sample block was taken out of the central part. To prevent the peak of hydration products from being covered by the peak of MS, the particle of MS in the sample block was removed. Then, the sample was ground into powder for XRD. All powder samples with a particle size of about 80 μm were soaked in anhydrous ethanol to stop the hydration reaction and dried in a vacuum drying oven at 60°C for 24 h before the experiment. Representing different hydration products in the four groups of samples, the peaks in the diffraction pattern were compared, and the hydration degree of samples could also be characterized.

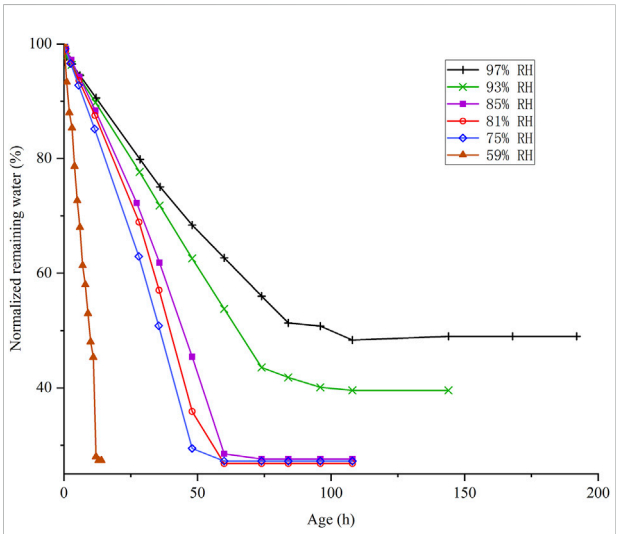

FIGURE 3
Desorption curve with time.

Thermal gravity analysis

Thermal gravity (TG) analysis is used to analyze the relative content of phases in a sample by the reduction in mass of samples at different temperatures (Deboucha et al., 2017; Chu et al., 2021). Also, it can be used to explore the chemistry binding water and calcium hydroxide content. The powder samples were placed in a vacuum drying environment, and TG curves of powder samples were measured with a rising temperature of 20–1050°C, a heating rate of 10°C/min, and an interval between data records of 0.1 s.

Scanning electron microscopy analysis

The microstructure of cement paste can be observed by using a scanning electron microscope (SEM). Samples cured for 28 days were smashed into uniform fragments with a flat fracture surface and about 1 cm in size. Then, fragments were immersed in an anhydrous ethanol solution to prevent the surface from being hydrated or carbonized. It should be noted that the samples should be dried in a vacuum drying oven at 60°C for 24 h before the experiment begins. In addition, the surface of samples was coated by low vacuum sputter Au to prevent the accumulation of static electric fields. Considering the desorption behavior of MS in specimens, the microstructure of the interfacial transition zone (ITZ) between MS and paste was mainly studied.

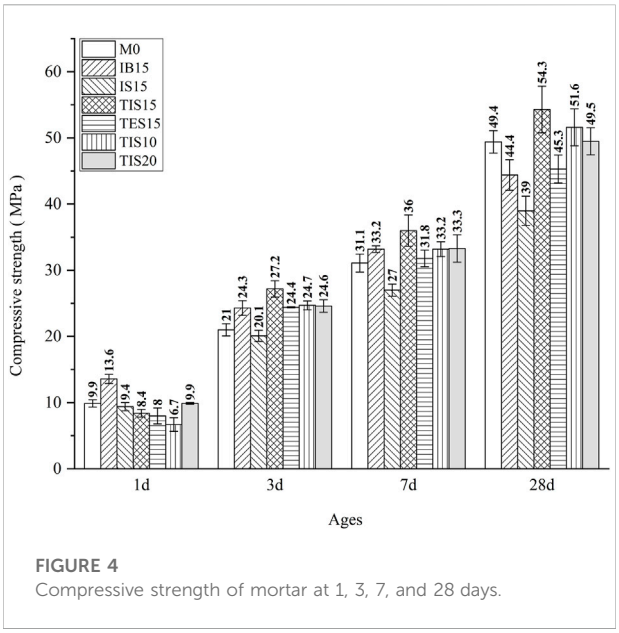

FIGURE 4
Compressive strength of mortar at 1, 3, 7, and 28 days.

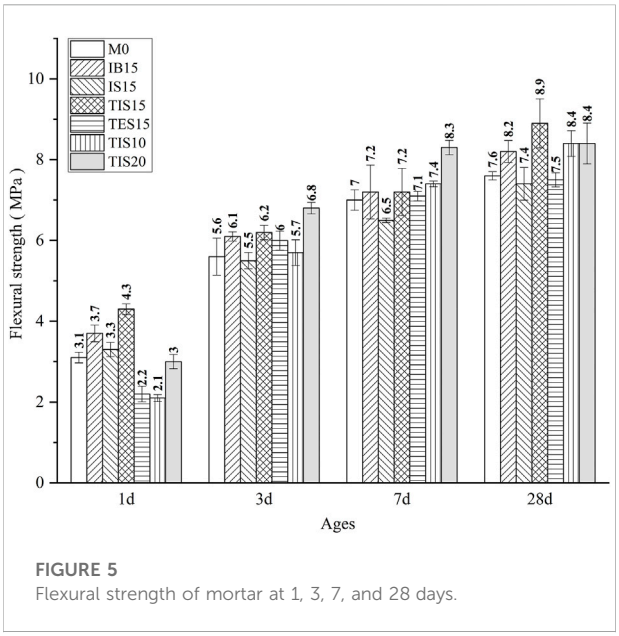

FIGURE 5
Flexural strength of mortar at 1, 3, 7, and 28 days.

Result

Desorption properties of the molecular sieve

The desorption curves of MS in different RH are shown in Figure 3. Before the curve reaches equilibrium, the change of internal moisture decreased linearly with time, which can also be found in the desorption curve of the other water storage materials, such as clay, bottom ash, shale, and SAP (Wang et al., 2015). The water release rates of MS increased with the reduction of RH, and it can be seen from the figure that the difference in the water release rate was small when RH was 85%, 81%, and 75%. Studies have shown that the water release rate is inversely proportional to the volume of water absorption and has no relation to the pore structure of the particles (Zou et al., 2018).

The final residual water content is also one of the important properties of the internal curing agent. The remaining water after the analytical curve reaches equilibrium will be left inside the molecular sieve and cannot be released. Then, 27% of water was left in the MS after water releasing. In addition, compared with other absorption aggregates in ASTM C1761/C1761M-12 (2012), residual equilibrium water absorption of MS was not ideal. Equilibrium water absorption has an important relationship with the pore structure (Zou et al., 2018). According to the information provided by the manufacturer, the pore size of MS was 0.9 nm. The pore size of MS was too small for water absorbed by MS to be released, which caused the residual water in MS to be higher than other absorbent lightweight aggregates.

Mechanical properties of mortar

Results of compressive and flexural strength at different ages are presented in Figures 4, 5. The strengths of three groups of mortars with the same content of MS (IB15, IS15, and TIS15) were compared. It can be seen, on days 3 and 7, that the compressive strength of group TIS15 was the highest, followed by those of groups IB15 and M0, and the strength of group IS15 was the lowest. The result was related to the actual water cement ratio in the initial stage of hardening. The actual water–cement ratio refers to the amount of water available for hydration and migration in the slurry at a given time, and the water inside the porous aggregate is not included because it cannot be consumed temporarily. Due to the humidity difference inside and outside MS, the free moisture in the slurry was absorbed into MS. Also, the desorption test showed that part of the absorbed water could not migrate out to participate in hydration. Thus, the actual water–cement ratio was decreased in the early stage of curing. On the contrary, the saturated MS continuously released water, and the actual water–cement ratio increased accordingly in IS15. According to the aforementioned observation, the initial actual water–cement ratio in group IS15 was the highest and those of the M0 group, IB15 group, and TIS15 group decreased successively. A small water–cement ratio obviously leads to a compact structure of the final cement paste and vice versa (Peng et al., 2022). The compressive strength decreased with a higher water–cement ratio (Schulze, 1999). This result was in accordance with the order of strength value in the figure. It could be seen that the influence of lightweight aggregates on mortar strength was not obvious in this period.

Notably, the 28-day strength of TIS15 was the highest. In all mix ratios, there are two groups of mix ratios that need to be

analyzed separately. Among M0, IB15, IS15, and TIS15 mortars, TIS15 has the highest strength. It is speculated that there are three factors causing this difference; they are the following:

1) The strength of mortar was affected by the water–cement ratio. The water absorption of the empty MS and the water release of the saturated MS led to the difference in the initial actual water–cement ratio in IB15 and IS15 mortars. It can be seen from the table of mix ratios that the initial water–cement ratio of TIS15 is the lowest, resulting in the higher strength of TIS15.
2) The lower strength of MS itself has a negative impact on the strength of the mortar. Many studies have shown that the higher porosity leads to a reduction in the strength of the water-absorbing lightweight aggregate itself, which negatively affects the later strength of concrete (Yang et al., 2021).
3) The strength of the paste was strengthened by internal curing water. With the decrease of the relative humidity in mortar, the water absorbed in MS would be released, replenishing the pore water. Compared with external curing, this internal curing water could improve the hydration degree of the cement paste in the central part of the specimens (Chidiac et al., 2021). Also, the compactness of the pore structure of paste was improved when the hydration products were accumulated in the pores (Sun et al., 2015). As a result, the strength of the paste was enhanced.

The initial water–cement ratio of IS15 was relatively high, while the internal curing effect of blank MS in IB15 was too small. The higher strength of TIS15 was the result of a combination of these three factors. The actual water–cement ratio was lower, leading to the higher strength, and the internal curing water in MS enhanced the hydration. The negative effects of MS were offset by the aforementioned two reasons in the TIS15 mixture.

Under the same total water content, TIS15 also has the highest strength in M0, TIS10, TIS15, and TIS20. The reasons are as follows:

1) It can be seen from the table of mix ratios that the order of the initial water–cement ratio is TIS20 < TIS15 < TIS10 < M0.
2) The curing efficiency increases with the increase of MS dosage. The migration distance of internal curing water is limited, which is about 2–4 mm according to reports (Yang et al., 2021). The smaller the distribution distance of the internal curing agent, the larger is the curing range of the curing water, and the better is the curing effect. Thus, the strength enhancement effect of internal curing was improved with the increase of MS.
3) The negative effect of MS on strength increases with the increase of dosage.

Finally, under the influence of the three factors, when the dosage was 15%, the strength was the highest.

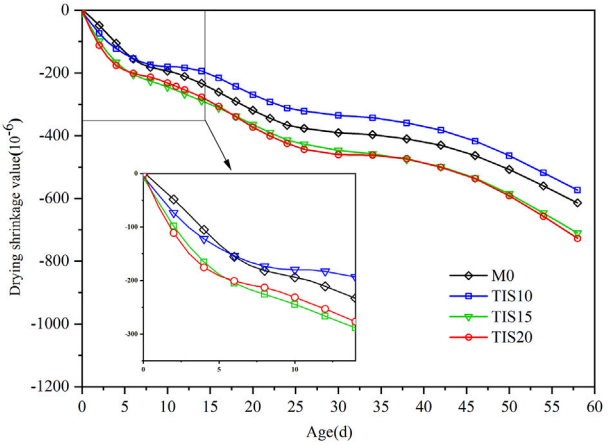

FIGURE 6
Drying shrinkage value curve with age.

It could be seen from the results that the mortar with the same total water content as M0 was stronger than those with additional water. Then, the strengths of four groups of mortars with the same total water content (TES15, TIS15, TIS10, and TIS20) were compared. Also, it could be seen that the internal mixing method may be more suitable for MS from the strength results of TIS15 and TES15. It was speculated that the appropriate incorporation method of molecular sieves in the mortar was as follows: *1*) the total water content is kept the same; *2*) the MS is mixed into the mortar by the internal mixing method. The strength of mortars M0, TIS10, TIS15, and TIS20 in accordance with the aforementioned conditions was compared and analyzed. The results showed that the compressive strength of mortars with the sand replacement volume of 10%, 15%, and 20% increased by 5%, 10%, and 0.2%, respectively, and the flexural strength increased by 10.5%, 17%, and 10.5%.

Drying shrinkage performance of mortar

The mortars with the same total water content and different MS replacement rates were tested. The curves of the dry shrinkage value with age are shown in Figure 6.

The drying shrinkage curve shows that the higher the dosage of MS was, the higher the growth rate was within the initial 2 days. At this time, the order of dry shrinkage values was as follows: TIS20 > TIS15 > TIS10 > M0. This may be related to the initial actual water–cement ratio in the mortar. The total water content of the four groups was the same, while the extra water carried by the MS was different. Thus, the order of the initial actual water–cement ratio was as follows: M0> TIS10 > TIS15 > TIS20. Drying shrinkage was attributed to the water loss from large pores of concrete in dry environments, which was one of the

primary reasons for the generation of cracks in concrete (Wang et al., 2022a). In addition, water was also continuously consumed in the hydration process of cement. With the reduction of free water in cement paste, the meniscus tension increased continuously, and shrinkage occurred when the liquid surface tension exceeded the tensile strength (Li et al., 2021). The earlier this critical state was reached, the less was the curing time of the cement paste, leading to the lower strength. Also, it further resulted in the earlier arrival of the critical state. Thus, the smaller the initial actual water–cement ratio, the earlier the critical state appeared, and the greater the shrinkage at the early stage. This was the same as the order of dry shrinkage value mentioned earlier.

In the next 8 days, compared with the control group, the drying shrinkage of TIS10, TIS15, and TIS20 was significantly alleviated, especially TIS20. This was closely related to the behavior of water migration in pre-absorbent MS. The internal curing water in MS supplemented pore water and reduced the liquid surface tension, which alleviated drying shrinkage. In addition, supplemented water could promote hydration reaction, and hydration products accumulated in paste pores, changing the pore structure in the paste. Also, it is well known that the pore structure strongly affects the mechanical properties, shrinkage behavior, and durability of concrete (Huang et al., 2021; Wang et al., 2022b).

It is worth noting that the larger the dosage, the more obvious is the alleviating effect. The curing effect of the internal curing agent was improved with the decrease in the distribution distance (Bentz and Snyder, 1999). Thus, the alleviating effect of shrinkage was most obvious in the TIS20 mortar. This alleviating effect disappeared around day 10 except for TIS10, which disappeared on day 15. It was speculated that it was caused by the initial actual water–cement ratio. Desorption experiments showed that the higher the relative humidity, the slower the water release rate was. Also, TIS10 had the highest initial actual water–cement ratio and the highest relative humidity, resulting in the slowest water release rate. Thus, saturated MS in TIS10 had the longest time to completely release water, and the duration of this alleviating effect in TIS10 was longer than that in TIS15 and TIS20.

It could be seen that the growth rate of the dry shrinkage value increased with the increase in the MS content after 40 days. This phenomenon was also mentioned in reference, and it may be related to the shrinkage of aggregates (Álvaro et al., 2021).

After 60 days of curing, the dry shrinkage value of TIS10 was the lowest and that of TIS15 and TIS20 were higher than M0 except for TIS10. There were four reasons for this result. On the one hand, according to the desorption curve, nearly 20% of absorbed water was still left in MS after releasing water. The higher the content of MS, the more water was left in MS. Although the total water content of the four groups was the same, the actual total available water for hydration and water migration was lower than M0, leading to greater shrinkage. On the other hand, the lower initial water–cement ratio intensified

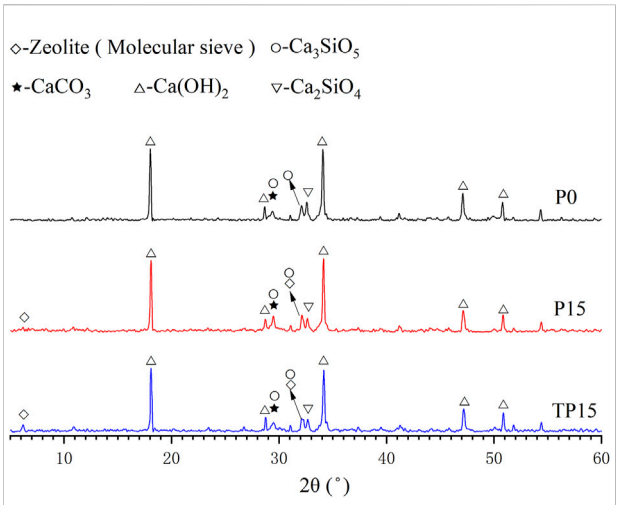

FIGURE 7
XRD patterns of pastes at 28 days.

the early drying shrinkage of mortar, leading to a higher early shrinkage value, especially TIS20, which even increased by more than 60% compared with M0. Also, because the concrete at an early age may have more connected pores leading to the loss of free water, most of the dry shrinkage of concrete occurs in the early dry shrinkage stage (Wang et al., 2021a). These two reasons will lead to the intensification of dry shrinkage deformation. However, as mentioned in the previous analysis, internal curing water in MS could alleviate shrinkage deformation. In addition, the addition of pre-saturated MS optimized the process of water loss and reduced water consumption of evaporation in a dry environment. It should be noted that although the available actual total water content in TIS10 was less than M0, the dry shrinkage value in 60 days was still reduced. The results of the drying shrinkage experiment were produced under the combined influence of these four reasons. Although drying shrinkage was effectively alleviated by the water supplement of saturated MS, early drying shrinkage deformation in TIS15 and TIS20 was too severe to be compensated. Under the same total water content, there was a suitable dosage, and the shrinkage experiment showed that the appropriate dosage was 10%.

The results show that the drying shrinkage value of TIS10 finally decreased by 6% and even decreased by 17.5% at the age of 30 days, while the compressive strength and flexural strength increased by 5% and 10.5%, respectively. Although the strength of TIS15 was higher than that of TIS10, the dry shrinkage value was decreased relative to M0.

XRD analysis

The XRD patterns of pastes are shown in Figure 7. It can be seen from the XRD patterns that no zeolite (MS) diffraction peak

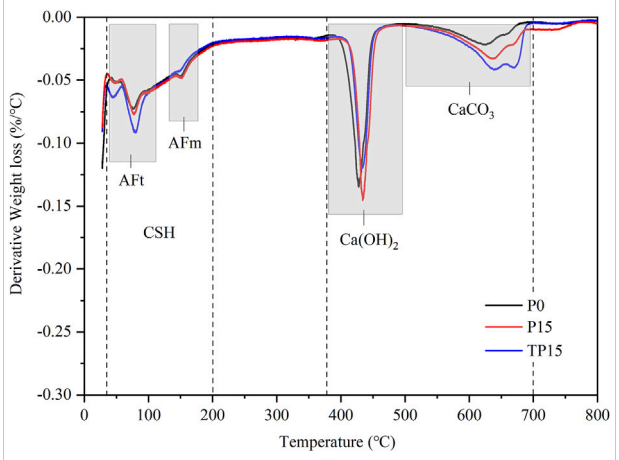

FIGURE 8
Results of TGA at 28 days: dehydration of C-S-H (40–200°C), dehydroxylation of CH (370–500°C), and decarbonization of calcium carbonate (500–700°C).

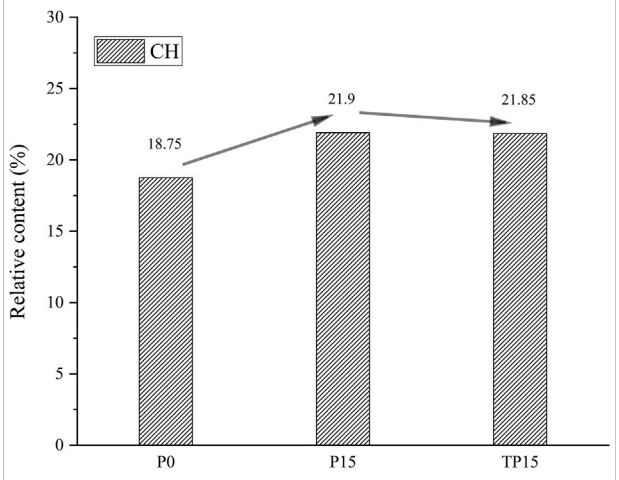

FIGURE 9
Relative content of CH in different samples.

was observed at 6–7° in P0 due to the absence of MS incorporation. There existed the same representative diffraction peaks of hydration products in all of the samples. The main compounds in the XRD patterns were $Ca(OH)_2$ (CH), unhydrated cement Ca_3SiO_5(C_3S), Ca_2SiO_4 (C_2S), and $CaCO_3$. CH is the condition for the formation of AFt and gypsum crystals (Yang et al., 2022a). Calcium silicate hydrate (C-S-H), one of the hydration products, was not found in any of the three samples, which is due to the ill-crystalline/amorphous nature of C-S-H (Salaheddine et al., 2016).

Hydration products' composition of paste was not altered after mixing MS. However, there existed an influence of MS on the intensity of hydration peaks, which was related to the degree of hydration in the paste. Also, the quantitative analysis of the hydration degree was mainly concentrated in TG analysis.

TG analysis

To compare the composition content of the four groups of cement paste, the derivative curve corresponding to thermogravimetric loss at the age of 28 days is shown in Figure 8. According to the derivative curve, it can be seen that there existed several peaks in the range of temperatures at 20–900°C, corresponding to the main mass loss in the TG curve, which represented the amount of the corresponding compositions in samples.

The first peak in the derivative curve appeared at about 80°C. Weightlessness occurs before 200°C due to the evaporation of physically bound water from ettringite (Aft) and calcium silicate hydrate (C-S-H) in samples (Kim et al., 2021). The strength of the cementitious material was increased by the production of these phases (Jeong et al., 2016). As can be seen from Figure 8, the relative content of evaporation water within 40–200°C in P15 and TP15 increased by 3% and 6%, respectively. Thus, it was speculated that the content of C-S-H was one of the reasons for the increase in mortar strength. In addition, the small peak at 150°C in this region could be related to the dehydration of the monosulfate (Jeong et al., 2020).

The second peak in the derivative curve appeared at about 430°C. Limited by the differences in instruments, conditions, and the specimen preparation process in the experiment, the decomposition of CH occurred at a different temperature range in studies by many scholars. But it was certain that the mass loss generally occurred at about 450°C (Vedalakshmi et al., 2003; Esteves et al., 2014; Lyu et al., 2020; Mao et al., 2021; Yang et al., 2022b). The third peak in the derivative curve appeared at about 640°C. It could be related to decarbonization of calcium carbonate ($CaCO_3$) (Wang et al., 2020; Wang et al., 2021b; Ahsen et al., 2022). To sum up, stages of peaks in the derivative curve represented dehydration of C-S-H, dehydration of CH, and decarbonization of $CaCO_3$, respectively. The ignition loss of each sample at different temperatures is shown in the Supplementary Material.

Hydration degree

The content of hydration products can reflect the degree of hydration (Kim et al., 2021). Also, the relative contents of CH are shown in Figure 9. The process of dehydration of CH may cover multiple temperature ranges for the reason that the material decomposed at each temperature stage is not a single substance (Lyu et al., 2020). Also, the carbonization of CH was one of the

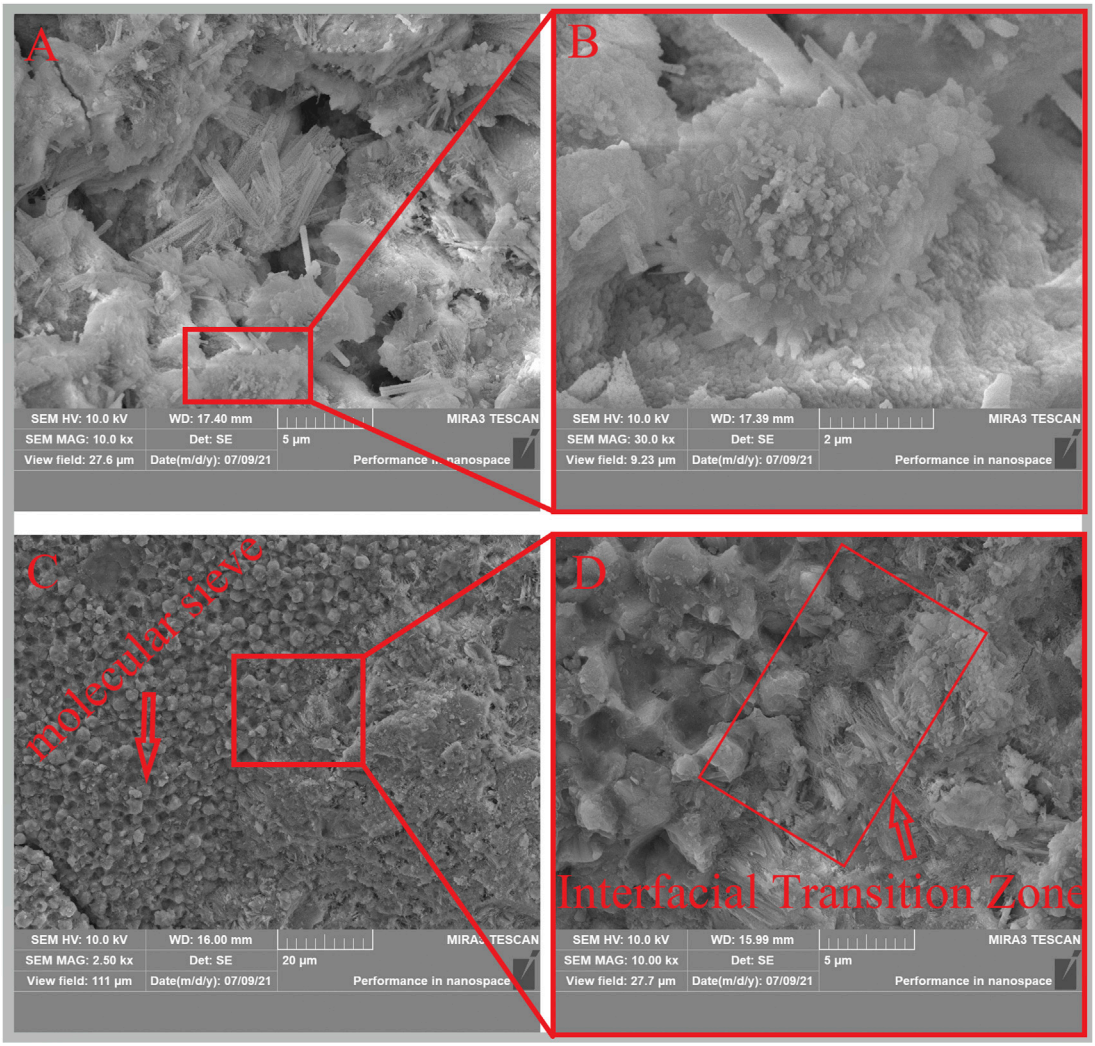

FIGURE 10
Morphology of different groups at 28 days: **(A,B)** is the morphology of sample P0; **(C,D)** is the morphology of sample TP15.

sources of $CaCO_3$ in samples. TG curves showed that the sample was carbonized during storage. The calculation method of the content of CH (m_{CH}) is based on the study of reference (Lyu et al., 2020), which is shown as follows:

$$m_{CH} = m_A \times \frac{M_{CH}}{M_{H_2O}} + m_B \times \frac{M_{CH}}{M_{CO_2}}, \tag{3}$$

where, m_A and m_B are the mass losses within temperatures at 370–500°C and 500–700°C, respectively, and M_{CH}, M_{CO_2}, and M_{H_2O} are the relative molecular masses.

The CH contents of P15 and TP15 increased by 29% and 28%, respectively. The content of hydration products could represent the hydration degree of paste to a certain extent (Lei et al., 2021). Thus, it can be inferred that the hydration degree of P15 was the highest, followed by TP15. Also, this result was consistent with the sequence of C-S-H relative contents. The hydration degree of cement-based materials was improved by the incorporation of saturated MS, which revealed the mechanism of mortar strength enhancement.

It is worth noting that the total water consumption in TP15 is the same as P0 and lower than P15. The desorption test of MS showed that 28% of water absorbed by saturated MS could not be released due to the small pores. Thus, the actual total water consumption of TP15 was even lower than P0. However, the hydration degree of TP15 exceeded P0. It was speculated that the MS reduced the initial water–cement ratio, slowed down the initial water volatilization in the paste, and reduced the water loss.

The analysis of mass loss demonstrated that the incorporation of MS into cement-based materials promoted

the hydration of cement-based materials. Also, it verified the speculations and conclusions of the early strength of mortar.

SEM analysis

The microscopic morphology of different samples is shown in Figure 10. The morphology of sample P0 is shown in Figures 10A,B. A large amount of granular C-S-H appeared in the microscopic image of the sample, which accumulated together to form cement stone and was the main contributor to the strength of paste (Tang et al., 2021), as shown in Figure 10B. There were also some columnar Aft interspersed among them, as shown in Figure 10A. However, there were pores less than 2 μm in diameter between them. The image of Figures 10C,D was taken from the interfacial transition region near the MS. It can be seen from the image that the MS had a rough surface, which was conducive to bonding with the paste. There was no obvious gap between the paste and MS. Both were connected by dense bundles Aft and C-S-H. This was related to the release of water from MS. In the process of water release, the humidity in the transition zone was always maintained at a high level. Thus, the hydration degree was higher than that in other regions. However, the MS was removed from the paste during the processing of the test sample. Thus, the contents of C-S-H and Aft in TGA were reduced due to the influence of the experimental operation. At the same magnification, owing to the enhanced hydration degree, the density of paste at the interface transition zone was higher than that of P0. Also, it was one of the mechanisms of paste strength improvement.

Conclusion

In this study, the effect of waste MS on mechanical properties, dry shrinkage properties, and micro properties of internally cured cement-based materials was systematically studied. The main conclusions were summarized as follows:

(1) The water release rate of MS increased with the decrease in relative humidity. MS had a higher water absorption capacity than the other internal curing agents. However, the residual water content of MS was also higher than that of the other internal curing agents due to the nanoscale pore size. According to the results of the drying shrinkage experiment and analysis of degree of hydration, the water desorption performance of MS can meet the requirements as an internal curing agent.
(2) According to the results of the strength test, the internal mixing method was more suitable as the mixing method of MS. The low strength of waste MS itself would adversely affect the strength of mortar. However, when the total water content in the mix ratio remains unchanged after adding saturated MS, mortar strength would exceed that of the blank control mortar, and the adverse effects of MS can be offset by internal curing.
(3) A suitable mixture ratio of mortar containing factory adsorption waste MS was found. When the total water content was unchanged and the content of saturated MS was 10%, the compressive and flexural strength of mortar increased by 5% and 10%, respectively, while the drying shrinkage value finally decreased by 6% and even decreased by 17.5% at the age of 30 days. Although compressive and flexural strength were the highest when the dosage was 15%, the dry shrinkage value increased compared with the blank control group. There was no necessary relationship between dry shrinkage and strength.
(4) Water-saturated waste MS had no effect on the physical composition of cement-based materials. According to the results of the TG test, hydration product content was increased even though the total water content was unchanged after the incorporation of saturated MS. It means that the hydration degree of cement-based materials had been strengthened under the influence of saturated MS. The increase of hydration products may be the mechanism of mortar strength enhancement. In addition, SEM images show that the hydration products are enriched in the transition zone near MS, which was consistent with the results of the TG test.

Data availability statement

The original contributions presented in the study are included in the article/Supplementary Material; further inquiries can be directed to the corresponding author.

Author contributions

PS: investigation, visualization, and writing—original draft. ZL: conceptualization, methodology, resources, and funding acquisition. XC: writing—review and editing, data curation, and validation. LZ: supervision and project administration. RH: resources.

Funding

This work was financially supported by the Department of Science and Technology of Hubei Province (grant number: 2021BCA130), the Hubei Key Laboratory of Water System

Science for Sponge City Construction (Wuhan University) (grant numbers: 2020-04), and the Hubei Provincial Department of Education (grant number: Q20201304).

Conflict of interest

Author XC is employed by the China Western Construction Academy of Building Materials Co., LTD, and author RH is employed by Hubei Chufeng Jianke Group Jingzhou Kaiyuan New Materials Limited by Share LTD.

The remaining authors declare that the research was conducted in the absence of any commercial or financial relationships that could be construed as a potential conflict of interest.

Publisher's note

All claims expressed in this article are solely those of the authors and do not necessarily represent those of their affiliated organizations, or those of the publisher, the editors, and the reviewers. Any product that may be evaluated in this article, or claim that may be made by its manufacturer, is not guaranteed or endorsed by the publisher.

Supplementary material

The Supplementary Material for this article can be found online at: https://www.frontiersin.org/articles/10.3389/fmats.2022.1003556/full#supplementary-material

References

Ahsen, M. H., Siddique, M. S., Farooq, S. H., Usman, M., Aleem, M. A. U., Hussain, M., et al. (2022). Mechanical behavior of high-strength concrete incorporating seashell powder at elevated temperatures. *J. Build. Eng.* 50, 104226. doi:10.1016/j.jobe.2022.104226

Álvaro, R. R., Paz, S. S., Fonteboa, B. G., Mas, V. F., and Paine, K. (2021). Waste-Based porous materials as water reservoirs for the internal curing of Concrete. *A Rev. Constr. Build. Mat.* 299, 124244. doi:10.1016/j.conbuildmat.2021.124244

Antunes, A., Faria, P., Silva, V., and Bras, A. (2019). Rice husk-earth based composites: A novel bio-based panel for buildings refurbishment. *Constr. Build. Mat.* 221, 99–108. doi:10.1016/j.conbuildmat.2019.06.074

ASTM C1761/C1761M-12 (2012). *Standard specification for lightweight Aggregate for internal curing of concrete*. West Conshohocken, Pennsylvania, United States: American Society for Testing Materials.

ASTM-E104 (2012). *Practice for maintaining constant relative humidity by means of aqueous solutions*. West Conshohocken, Pennsylvania, United States: American Society for Testing Materials.

Balapour, M., Zhao, W., Garboczi, E. J., Oo, N. Y., Farnam, Y., Hsuan, Y. G., et al. (2019). Potential use of lightweight aggregate (LWA) produced from bottom coal ash for internal curing of concrete systems. *Cem. Concr. Compos.* 105, 103428. doi:10.1016/j.cemconcomp.2019.103428

Bentur, A., Igarashi, S. I., and Kovler, K. (2001). Prevention of autogenous shrinkage in high-strength concrete by internal curing using wet lightweight aggregates. *Cem. Concr. Res.* 31, 1587–1591. doi:10.1016/S0008-8846(01)00608-1

Bentz, D. P., Lura, P., and Roberts, J. W. (2005). Mixture proportioning for internal curing. *Concr. Int.* 27, 35–40.

Bentz, D. P., and Snyder, K. A. (1999). Protected paste volume in concrete: Extension to internal curing using saturated lightweight fine aggregate. *Cem. Concr. Res.* 29, 1863–1867. doi:10.1016/S0008-8846(99)00178-7

Bentz, D. P., and Weiss, W. J. (2011). *Internal curing: A 2010 state-of-the-art review*. Gaithersburg: US Department of Commerce, National Institute of Standards and Technology. doi:10.1016/j.jvcir.2009.09.004

Chidiac, S. E., Mihaljevic, S. N., Krachkovskiy, S. A., and Goward, G. R. (2021). Efficiency measure of SAP as internal curing for cement using NMR & MRI. *Constr. Build. Mat.* 278, 122365. doi:10.1016/j.conbuildmat.2021.122365

Chu, D. C., Kleib, J., Amar, M., Amar, M., Benzerzour, M., and Abriak, N. E. (2021). Determination of the degree of hydration of Portland cement using three different approaches: Scanning electron microscopy (SEM-BSE) and Thermogravimetric analysis (TGA). *Case Stud. Constr. Mater.* 15, e00754. doi:10.1016/j.cscm.2021.e00754

Deboucha, W., Leklou, N., Khelidj, A., and Oudjit, M. N. (2017). Hydration development of mineral additives blended cement using thermogravimetric analysis (TGA): Methodology of calculating the degree of hydration. *Constr. Build. Mat.* 146, 687–701. doi:10.1016/j.conbuildmat.2017.04.132

Dixit, A., Gupta, S., Pang, S. D., and Kua, H. W. (2019). Waste Valorisation using biochar for cement replacement and internal curing in ultra-high performance concrete. *J. Clean. Prod.* 238, 117876. doi:10.1016/j.jclepro.2019.117876

Esteves, L. P., Lukošiūtė, I., and Čėsnienė, J. (2014). Hydration of cement with superabsorbent polymers. *J. Therm. Anal. Calorim.* 118, 1385–1393. doi:10.1007/s10973-014-4133-4

Fajula, F., and Plee, D. (1994). Application of molecular sieves in view of cleaner technology. Gas and liquid phase separations. *Stud. Surf. Sci. Catal.* 85, 633–651. doi:10.1016/S0167-2991(08)60780-6

Ghourchian, S., Wyrzykowski, M., Lura, P., Shekarchi, M., and Ahmadi, B. (2013). An investigation on the use of zeolite aggregates for internal curing of concrete. *Constr. Build. Mat.* 40, 135–144. doi:10.1016/j.conbuildmat.2012.10.009

Huang, J. S., Li, W. W., Huang, D. S., Wang, L., Chen, E., Wu, C. Y., et al. (2021). Fractal analysis on pore structure and hydration of magnesium oxysulfate cements by first principle, thermodynamic and microstructure-based methods. *Fractal Fract.* 5, 164–181. doi:10.3390/fractalfract5040164

Igarashi, S. I., and Watanabe, A. (2006). "Experimental study on prevention of autogenous deformation by internal curing using super-absorbent polymer particles," in International RILEM Conference on Volume Changes of Hardening Concrete: Testing and Mitigation, Editor O. M. Jensen (FL: RILEM Publications SARL), 77–86. doi:10.1617/2351580052.009

Jensen, O. M., and Hansen, P. F. (2001). Water-entrained cement-based materials. *Cem. Concr. Res.* 31, 647–654. doi:10.1016/S0008-8846(01)00463-X

Jensen, O. M., and Lura, P. (2006). Techniques and materials for internal water curing of concrete. *Mat. Struct.* 39, 817–825. doi:10.1617/s11527-006-9136-6

Jeong, Y., Kang, S. H., Min, O. K., and Moon, J. (2020). Acceleration of cement hydration by hydrophobic effect from supplementary cementitious materials: Performance comparison between silica fume and hydrophobic silica. *Cem. Concr. Compos.* 112, 103688. doi:10.1016/10.1016/j.cemconcomp.2020.103688

Jeong, Y., Park, H., Jun, Y., Jeong, J. H., and Oh, J. E. (2016). Influence of slag characteristics on strength development and reaction products in a CaO-activated slag system. *Cem. Concr. Compos.* 72, 155–167. doi:10.1016/j.cemconcomp.2016.06.005

Justs, J., Wyrzykowski, M., Bajare, D., and Lura, P. (2015). Internal curing by superabsorbent polymers in ultra-high performance concrete. *Cem. Concr. Res.* 76, 82–90. doi:10.1016/j.cemconres.2015.05.005

Kawashima, S., and Shah, S. P. (2011). Early-age autogenous and drying shrinkage behavior of cellulose fiber-reinforced cementitious materials. *Cem. Concr. Compos.* 33, 201–208. doi:10.1016/j.cemconcomp.2010.10.018

Kim, S., Lee, N., Lee, H. K., and Park, S. (2021). Experimental and theoretical studies of hydration of ultra-high performance concrete cured under various curing conditions. *Constr. Build. Mat.* 278, 122352. doi:10.1016/j.conbuildmat.2021.122352

Kulkarni, S. J. (1998). Recent trends in the applications of zeolites and molecular sieves for the synthesis of speciality and fine chemicals. *Stud. Surf. Sci. Catal.* 113, 151–161. doi:10.1016/S0167-2991(98)80282-6

Lei, W., Jin, M., Wu, Y., Zhou, Y., and Tang, S. (2021). Hydration, shrinkage, pore structure and fractal dimension of silica fume modified low heat Portland cement-based materials. *Constr. Build. Mat.* 272, 121952. doi:10.1016/j.conbuildmat.2020.121952

Li, Y., Zhang, H., Huang, M. H., Yin, H. B., Jiang, K., Xiao, K. T., et al. (2021). Influence of different alkali sulfates on the shrinkage, hydration, pore structure, fractal dimension and microstructure of low-heat Portland cement, medium-heat Portland cement and ordinary Portland cement. *Fractal Fract.* 5, 79–106. doi:10.3390/fractalfract5030079

Liu, J., Shi, C., Ma, X., Khayat, K. H., Zhang, J., and Wang, D. (2017). An overview on the effect of internal curing on shrinkage of high performance cement-based materials. *Constr. Build. Mat.* 146, 702–712. doi:10.1016/j.conbuildmat.2017.04.154

Lv, Y., Ye, G., and Schutter, G. D. (2019). Utilization of miscanthus combustion ash as internal curing agent in cement-based materials: Effect on autogenous shrinkage. *Constr. Build. Mat.* 207, 585–591. doi:10.1016/j.conbuildmat.2019.02.167

Lyu, Z., Shen, A., Mo, S., Chen, Z., Qin, X., Li, D., et al. (2020). Life-cycle crack resistance and micro characteristics of internally cured concrete with superabsorbent polymers. *Constr. Build. Mat.* 259, 119794. doi:10.1016/j.conbuildmat.2020.119794

Mao, Z., Zhang, J., Luo, Z., Ma, Q., Duan, Y., Li, S., et al. (2021). Behavior evaluation of hybrid fibre-reinforced reactive powder concrete after elevated temperatures. *Constr. Build. Mat.* 306, 124917. doi:10.1016/j.conbuildmat.2021.124917

National Standard of the People's Republic of China (2004). *Method of testing Cements-Determination of strength*. GB/T17671-1999. Chinese.

National Standard of the People's Republic of China (2009). *Standard for test method of performance on building mortar*. JGJ/T70—2009. Chinese.

Peng, Y., Tang, S. W., Huang, J. S., Tang, C., Wang, L., and Liu, Y. F. (2022). Fractal analysis on pore structure and modeling of hydration of magnesium phosphate cement paste. *Fractal Fract.* 6, 337–355. doi:10.3390/fractalfract6060337

Pietro, L., Bentz, D. P., Lange, D. A., Kovler, K., and Bentur, A. (2004). "Pumice aggregates for internal water curing. in PRO 36: Proc.," in *Int. RILEM Symp. on Concrete Science and Engineering : A Tribute to Arnon Bentur* (Northwestern University, Evanston, IL, United States: Rilem publications), 137–151.

Pujado, P. R., Rabo, J. A., Antos, G. J., and Gembicki, S. A. (1992). Industrial catalytic applications of molecular sieves. *Catal. Today* 13, 113–141. doi:10.1016/0920-5861(92)80191-o

Ranjbar, S. (2013). *Effect of pre-wetted perlite and fibers on autogenous and plastic shrinkage of high strength concrete*. British Columbia, Canada: Diss. University of British Columbia. doi:10.14288/1.0073615

Salaheddine, A., Frank, W., Baptiste, J., Champenois, F., Hesselbarth, B., and Lothenbach, B. (2016). Chemical activation of hybrid binders based on siliceous fly ash and Portland cement. *Cem. Concr. Compos.* 66, 10–23. doi:10.1016/j.cemconcomp.2015.11.003

Schulze, J. (1999). Influence of water-cement ratio and cement content on the properties of polymer-modified mortars. *Cem. Concr. Res.* 29, 909–915. doi:10.1016/S0008-8846(99)00060-5

Sun, X., Zhang, B., Dai, Q. L., and Yu, X. (2015). Investigation of internal curing effects on microstructure and permeability of interface transition zones in cement mortar with SEM imaging, transport simulation and hydration modeling techniques. *Constr. Build. Mat.* 76, 366–379. doi:10.1016/j.conbuildmat.2014.12.014

Tang, S., Wang, Y., Geng, Z., Xu, X., Yu, W., HuBao, A., et al. (2021). Structure, fractality. Mechanics and durability of calcium silicate hydrates. *Fractal Fract.* 5, 47–80. doi:10.3390/fractalfract5020047

Van, V. T. A., Rößler, C., Bui, D. D., and Ludwig, H. M. (2014). Rice husk ash as both pozzolanic admixture and internal curing agent in ultra-high performance concrete. *Cem. Concr. Compos.* 53, 270–278. doi:10.1016/j.cemconcomp.2014.07.015

Vedalakshmi, R., Raj, A. S., Srinivasan, S., and Babu, K. G. (2003). Quantification of hydrated cement products of blended cements in low and medium strength concrete using TGA and DTA technique. *Thermochim. Acta.* 407, 49–60. doi:10.1016/S0040-6031(03)00286-7

Wang, F., Yang, J., Cheng, H., Wu, J., and Liang, X. (2015). Study on mechanism of desorption behavior of saturated superabsorbent polymers in concrete. *ACI Mat. J.J* 112, 463–469. doi:10.14359/51686996

Wang, L., Guo, F. X., Lin, Y. Q., Yang, H. M., and Tang, S. W. (2020). Comparison between the effects of phosphorous slag and fly ash on the C-S-H structure, long-term hydration heat and volume deformation of cement-based materials. *Constr. Build. Mat.* 250, 118807. doi:10.1016/j.conbuildmat.2020.118807

Wang, L., Jin, M. M., Wu, Y. H., Zhou, Y. X., and Tang, S. W. (2021). Hydration, shrinkage, pore structure and fractal dimension of silica fume modified low heat Portland cement-based materials. *Constr. Build. Mat.* 272, 121952–121964. doi:10.1016/j.conbuildmat.2020.121952

Wang, L., Li, G., Li, X., Guo, F., Tang, S. W., Lu, X., et al. (2022). Influence of reactivity and dosage of MgO expansive agent on shrinkage and crack resistance of face slab concrete. *Cem. Concr. Compos.* 126, 104333–104345. doi:10.1016/j.cemconcomp.2021.104333

Wang, L., Luo, R. Y., Zhang, W., Jin, M. M., and Tang, S. W. (2021). Effects of fineness and content of phosphorus slag on cement hydration, permeability, pore structure and fractal dimension of concrete. *Fractals* 29, 2140004. doi:10.1142/S0218348X21400041

Wang, L., Yu, Z. Q., Liu, B., Zhao, F., Tang, S. W., and Jin, M. M. (2022). Effects of fly ash dosage on shrinkage, crack resistance and fractal characteristics of face slab concrete. *Fractal Fract.* 6, 335–354. doi:10.3390/fractalfract6060335

Xu, F., Lin, X., and Zhou, A. (2021). Performance of internal curing materials in high-performance concrete: A review. *Constr. Build. Mat.* 311, 125250. doi:10.1016/j.conbuildmat.2021.125250

Yang, H. M., Zhang, S. M., Lei, W., Chen, P., Shao, D. K., Tang, S. W., et al. (2022). High-ferrite Portland cement with slag: Hydration, microstructure, and resistance to sulfate attack at elevated temperature. *Cem. Concr. Compos.* 130, 104560. doi:10.1016/j.cemconcomp.2022.104560

Yang, H. M., Zhang, S. M., Wang, L., Chen, P., Shao, D. K., Tang, S. W., et al. (2022). High-ferrite Portland cement with slag: Hydration, microstructure, and resistance to sulfate attack at elevated temperature. *Cem. Concr. Compos.* 130, 104560. doi:10.1016/j.cemconcomp.2022.104560

Yang, L., Shi, C., Liu, J., and Wu, Z. (2021). Factors affecting the effectiveness of internal curing: A review. *Constr. Build. Mat.* 267, 121017. doi:10.1016/j.conbuildmat.2020.121017

Ye, G., Breugel, K. V., Lura, P., and Mechtcherine, V. (2012). *Application of super absorbent polymers (SAP) in concrete construction*. Dordrecht, Netherlands: Springer Netherlands.

Zhuang, Y. Z., Zheng, D. D., Ng, Z., Ji, T., and Chen, X. F. (2016). Effect of lightweight aggregate type on early-age autogenous shrinkage of concrete. *Constr. Build. Mat.* 120, 373–381. doi:10.1016/j.conbuildmat.2016.05.105

Zou, D., Li, K., Li, W., Li, H., and Cao, T. (2018). Effects of pore structure and water absorption on internal curing efficiency of porous aggregates. *Constr. Build. Mat.* 163, 949–959. doi:10.1016/j.conbuildmat.2017.12.170